ACS OMEGA

http://pubs.acs.org/journal/acsodf

Article

Oxygen Reduction Reaction with Manganese Oxide Nanospheres in Microbial Fuel Cells

Bhuvan Vemuri, Govinda Chilkoor, Pramod Dhungana, Jamil Islam, Aravind Baride, Nikhil Koratkar, Pulickel M. Ajayan, Muhammad M. Rahman, James D. Hoefelmeyer,* and Venkataramana Gadhamshetty*

Cite This: *ACS Omega* 2022, 7, 11777−11787

Read Online

ACCESS | Metrics & More | Article Recommendations | Supporting Information

ABSTRACT: Operating microbial fuel cells (MFCs) under extreme pH conditions offers a substantial benefit. Acidic conditions suppress the growth of undesirable methanogens and increase redox potential for oxygen reduction reactions (ORRs), and alkaline conditions increase the electrocatalytic activity. However, operating any fuel cells, including MFCs, is difficult under such extreme pH conditions. Here, we demonstrate a pH-universal ORR ink based on hollow nanospheres of manganese oxide (h-Mn_3O_4) anchored with multiwalled carbon nanotubes (MWCNTs) on planar and porous forms of carbon electrodes in MFCs (pH = 3−11). Nanospheres of h-Mn_3O_4 (diameter ∼ 31 nm, shell thickness ∼ 7 nm) on a glassy carbon electrode yielded a highly reproducible ORR activity at pH 3 and 10, based on rotating disk electrode (RDE) tests. A phenomenal ORR performance and long-term stability (∼106 days) of the ink were also observed with four different porous cathodes (carbon cloth, carbon nanofoam paper, reticulated vitreous carbon, and graphite felt) in MFCs. The ink reduced the charge transfer resistance (R_{ct}) to the ORR by 100-fold and 45-fold under the alkaline and acidic conditions, respectively. The current study promotes ORR activity and subsequently the MFC operations under a wide range of pH conditions, including acidic and basic conditions.

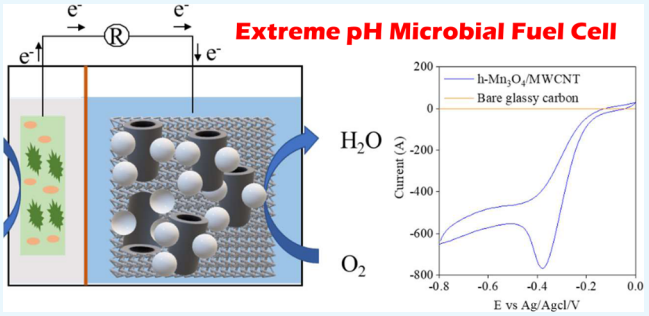

INTRODUCTION

Oxygen reduction reactions (ORRs) sustain performances of living systems (e.g., plants, algal cells) and energy harvesting fuel cell devices including microbial fuel cells (MFCs). MFCs use electrochemically active microorganisms (exoelectrogens) for converting organic matter in waste streams into direct current(DC) electricity. Although advanced designs involve a stack of rectangular or vertical modules with interchangeable cassette electrodes, a basic MFC unit consists of an anode (e^- donor: organic matter), cathode (e^- acceptor: oxygen), and optional membrane. A bottleneck to MFC operation includes high overpotential and sluggish ORR kinetics on the cathode surfaces. Catalysts based on platinum-group metals can effectively overcome these challenges. However, their high costs restrict their use to automobiles and space mission applications.

Operating MFCs under extreme pH conditions offers a substantial benefit. Such MFCs treat *acidic* wastes from mining, anaerobic digestors, and distillery wastewater, as well as *alkaline* wastes from manufacturing processes (e.g., animal hide, paper, and cement products) and electroplating industry.[1−5] Acidic conditions (pH < 4.0) suppress the growth of methanogens, expand the pH gradient, and accelerate the charge transport (proton) through the cation exchange membranes (e.g., p*K*a for protonated perfluorinated sulfonic acid in Nafion is less than one). Acidic conditions increase redox potential for the ORRs (+59 mV for each pH unit reduction). On the other hand, alkaline conditions increase electrocatalytic activity and enable the use of a range of affordable materials for fabricating MFC components (e.g., bipolar plates, membranes).

It is difficult to operate any fuel cells, including MFCs, under extreme pH conditions. The anode and cathode compartments are ionically connected through the ion exchange membranes. Thus, the extreme pH conditions in the anode can alter pH conditions in the cathode. The resulting membrane pH gradient, caused by the acidification of the anode and alkalization of the cathode, imposes operational challenges. Alkaline conditions create OH^- that adsorbs onto the cathode surfaces, blocking the O_2 adsorption as well as promoting the outer-sphere electron-transfer mechanism, resulting in an

Received: December 8, 2021
Accepted: February 25, 2022
Published: April 1, 2022

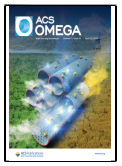

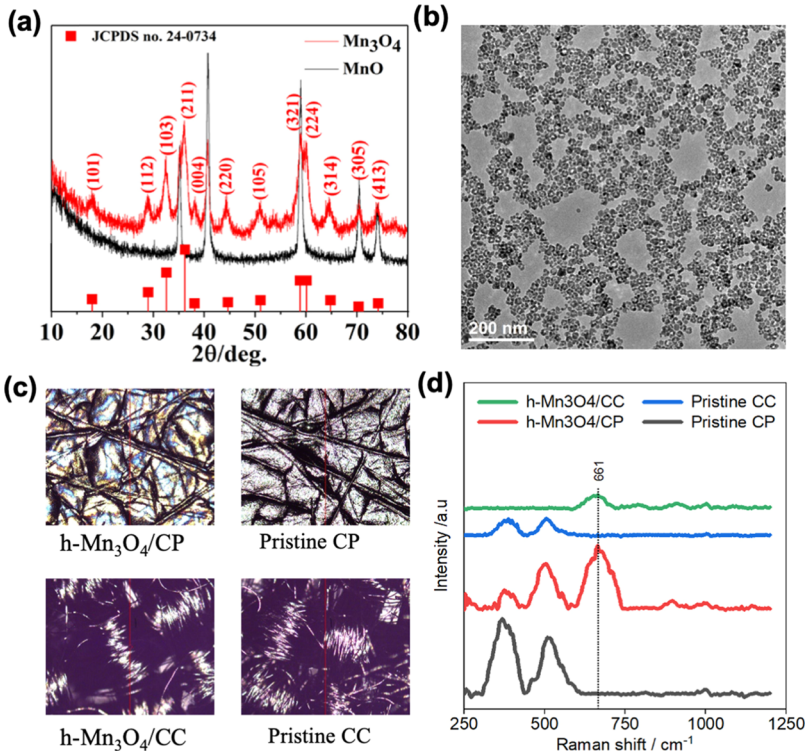

Figure 1. (a) PXRD shows the relevant peaks for Mn_3O_4, (b) TEM image of h-Mn_3O_4 crystal, (c) optical spectroscopy images at 10× magnification, and (d) Raman spectroscopy.

undesirable $2e^-$ peroxide as an intermediate.[6] CO_2 dissolves in alkaline environments, including those in hydrated anion exchange membranes (AEMs), causing cell carbonation and voltage losses (100−400 mV).[7] There is a clear need to develop a pH-universal catalyst for sustaining ORR reactions under extreme pH conditions for MFC applications (pH = 3−10).

Earth-abundant materials, M−N−C materials, where M = earth-abundant transition metals (e.g., nickel and manganese), N = nitrogen, C = carbon, can yield viable ORR catalysts for MFC applications. Catalysts based on the Mn_xO_y nanoparticles have emerged as attractive choices for electrochemical devices.[8−13] The Mn_xO_y nanoparticles can be obtained in various shapes and sizes, as needed by the devices.[14−16] We present a first study that explores the ORR activity of hollow h-Mn_3O_4 nanospheres[17,18] under extreme conditions in MFCs. We present a scalable route for synthesizing the ink based on nanospheres, anchor them with MWCNTs, and deposit them on diverse electrodes, including a planar glassy carbon and four porous carbon electrodes. A series of electrochemistry tests based on RDE and MFCs was used to assess the ORR performances. Microscopy and spectroscopy tests, rotating disk electrode (RDE) tests, electrochemical impedance spectroscopy analysis, and MFC tests were used to assess the long-term stability and the ORR performance of the ink under extreme pH conditions.

RESULTS AND DISCUSSION

We synthesized nanospheres of h-Mn_3O_4 using the Kirkendall growth process and anchored onto the MWCNTs in the presence of Nafion (herein referred to as catalyst ink). The commercially available carbon electrodes, including glassy carbon, graphite felt (GF), reticulated vitreous carbon (RVC), carbon cloth (CC), and carbon paper (CP), were modified with the catalyst ink and vacuum-dried at 200 °C. Details of the synthesis of MnO, h-Mn_3O_4 nanocrystals, ink, and coated electrodes are discussed in the later sections. As seen in the powder X-ray diffraction (PXRD) data (Figure 1a), the as-synthesized MnO particles were converted effectively into the h-Mn_3O_4 particles (hausmannite, JCPDS card no. 24-0734). Our earlier studies demonstrated the hollow morphology of the h-Mn_3O_4 nanospheres based on the high-angle annular dark-field scanning transmission electron microscopy (HAADF-STEM) and TEM image analyses (Figure 1b). These nanospheres were characterized by an inner diameter of ∼20 nm, outer diameter of 30−40 nm, and shell thickness of ∼7 nm.[17,18] An immediate application of as-synthesized ink is its use as a noninvasive coating to promote the ORR activity of carbon electrodes in MFCs. As seen in Figure 2, both the planar and porous forms of electrodes were amenable to the modification by the ink. Considering the diverse surface properties of these electrodes (see Table 1 for key surface properties), these findings indicate the use of ink for a diverse range of electrodes. As shown in the optical images for the CP, CC, h-Mn_3O_4/CP, and h-Mn_3O_4/CC, the coated and uncoated electrodes displayed distinct differences in terms of light interferences (Figure 1c). However, they displayed a varying degree of adsorption of nanoparticles and subsequently different ORR performances. These differences are due to the differences in their key surface properties. For instance, the light interference for h-Mn_3O_4/CP was more noticeable than that for h-Mn_3O_4/CC, which can be attributed to the greater adsorption in the CP electrode. The percentage of Mn on the surfaces of CC, RVC, and CP electrodes was 0.297, 0.036, and ∼2%, respectively, based on the elemental analysis using the ICP-AES techniques (Figure S3, Supporting Information). The adsorption by the CP electrode was 6.7 times and 55.5 times

https://doi.org/10.1021/acsomega.1c06950
ACS Omega 2022, 7, 11777−11787

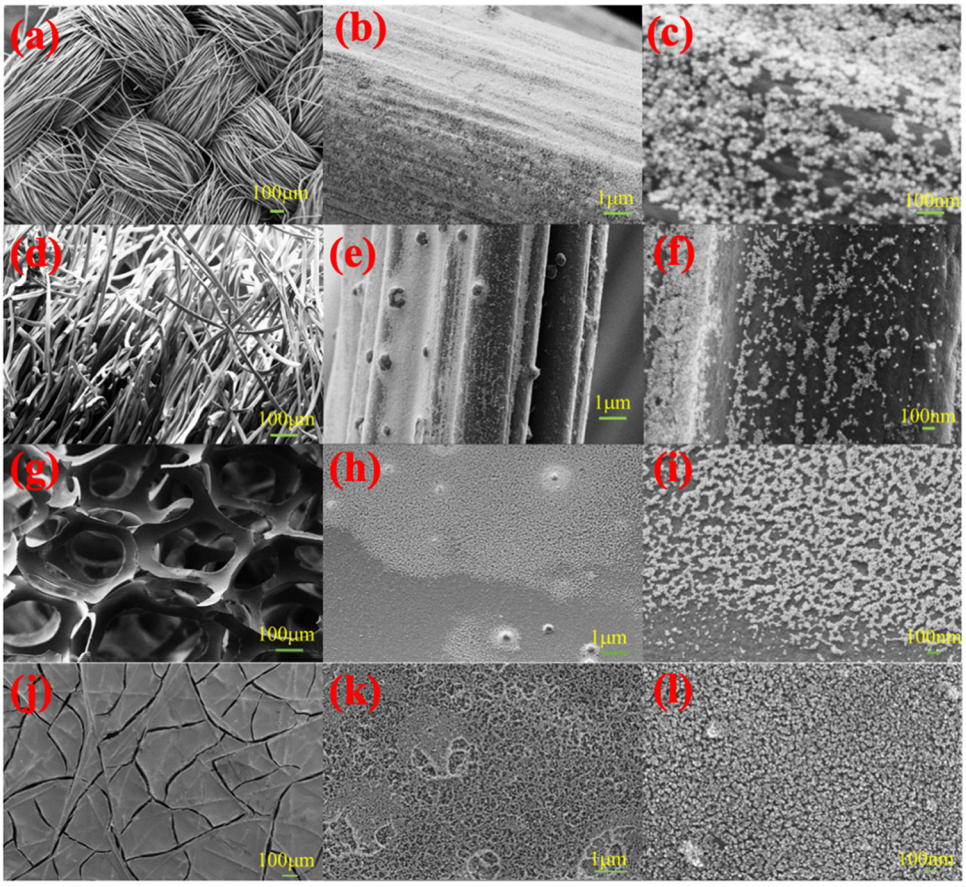

Figure 2. SEM images of the carbon electrodes modified with the catalyst ink (a) CC at lower magnification; scale bar: 100 μm (b,c) at higher magnification; scale bar: 1 μm and 100 nm; (d) graphite felt at lower magnification; scale bar: 100 μm (e,f) at higher magnification; scale bar: 1 μm and 100 nm; (g) RVC at lower magnification; scale bar: 100 μm (h,i) at higher magnification; scale bar: 1 μm and 100 nm. (j) Carbon nanofoam paper at lower magnification; scale bar: 100 μm (k,l) at higher magnification; scale bar: 1 μm and 100 nm.

Table 1. Summary of the Key Electrode Surface Properties

electrode	pore size	specific surface area (m^2/g)	contact angle	electrical conductivity (S/m)	ref
carbon cloth (CC)	10−31 mm	>1000	∼127°	∼623	22,23
graphite felt (GF)	3.5−15 nm	>0.7	∼120°	∼200 to 250	24−27
reticulated vitreous carbon (RVC)	5−100 pores/inch	>300	∼74°	∼370	28−30
carbon nanofoam paper (CP)	0.7−0.8 nm	400−600	∼90°	5000−23,000	31

greater than CC and RVC, respectively, as corroborated by the Raman studies (Figure 1c). The CP electrode displayed a broader Raman band with higher intensity compared with CC electrode (Figure 1c). Both the CC and CP electrodes displayed a vibrational Raman band at 661 cm^{-1} that corresponds to h-Mn_3O_4.[19,20] The pristine CP and CC electrodes did not display these peaks (Figure 1d). The greater coverage on the surface of the CP and CC, compared with the RVC, is due to their lower void space (measured in terms of pore size), higher contact angle, and lower specific area (Table 1). For example, the pore size of the CP electrode (0.7 nm) is 15-fold higher than that of the CC electrode (10 nm).

Their interfacial properties influence heterogeneous catalytic reactions between reactants and catalyst surfaces. The wettability affects the molecular diffusion rates of O_2 and the subsequent ORR performance of the electrode. To examine the influence of the ink on the wettability of the CP and CC electrodes, we measured their static contact angles using a sessile drop technique (Figure S1, Supporting Information). Upon coating with the ink, the contact angle of the CP electrode decreased from 90° to 0°, yielding a super hydrophilic surface. The contact angle for the pristine CC electrode was ∼122° (hydrophobic), which reduced only slightly after coating it with the ink. Generally, hydrophilic surfaces enhance the adsorption of O_2 and overall ORR kinetics.[21] Based on the above results, we have selected h-Mn_3O_4/CC and h-Mn_3O_4/CP electrodes as promising candidates for aqueous air-cathodes in our MFC studies.

ORR Performance of Coated Glassy Carbon (GC) Electrodes (Abiotic Conditions). The bare GC electrode did not show any ORR peaks under the N_2-O_2-saturated conditions (Figure S4, Supporting Information). The coated GC electrode did not register any ORR peaks under the N_2-saturated conditions (Figure S5, Supporting Information). However, it yielded a distinct O_2 reduction peak (0.45 V vs Ag/AgCl) under the O_2-saturated conditions (Figure 3), suggesting the conspicuous catalytic activity of the ink toward ORR. The reduction peak lay within −0.4 to −0.45 V (vs Ag/Ag/Cl) for all the scan rates. The limiting currents increased

https://doi.org/10.1021/acsomega.1c06950
ACS Omega 2022, 7, 11777−11787

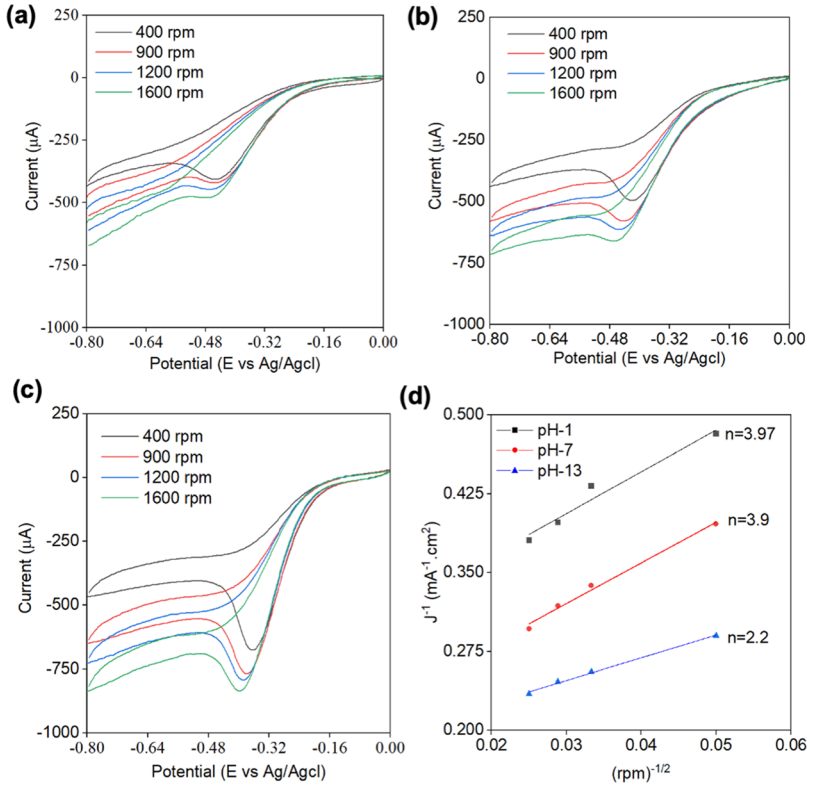

Figure 3. The ORR performance of glassy carbon electrodes modified with h-Mn_3O_4/MWCNTs ink. Rotating disk cyclic voltammograms under O_2-saturated conditions: (a) 0.1 M H_2SO_4 (pH 1), (b) 0.01 M KCl (pH 7), (c) 0.1 M KOH (pH 13) with a sweep rate of 50 mV/s, and (d) Koutecky–Levich plots at pH 1,7 and 13 with a linear fit.

with the increasing rotating speeds at all three pH conditions. For example, at pH-1, the limiting current at 1600 rpm (563 μA) was 1.9-fold higher compared with 400 rpm (514 μA) (Figure 3a). The Koutecky–Levich (K–L) plots (J^{-1} vs ω^{-1}) were used to determine the number of electrons (n) involved in the ORRs (Figure 3d). The linearity of the K–L plots indicated first-order rate kinetics toward the O_2 concentration (Figure 3d). Based on the analyses of the K–L plots, the values of the average electron-transfer number were found to be 3.97, 3.9, and 2.2. at pH 1, pH 7, and pH 13, respectively. Unlike the $2e^-$ pathway, the $4e^-$ pathway minimizes the formation of hydrogen peroxide and yields higher energy conversion efficiency. These results indicate that the h-Mn_3O_4/MWCNT ink works effectively under acidic and neutral conditions.

ORR Performance of the Ink on Cathodes in MFCS under Neutral pH Conditions. After assessing the performance of the ink under well-controlled RDE conditions on a bench scale, we tested its performance on the porous cathode materials (CP, CC, GF, and RVC) in MFC prototypes (Figure 4). We demonstrate the long-term performance of the ink under neutral conditions and latter under extreme pH conditions. The net performance of the MFCs was evaluated by monitoring temporal profiles of the operating voltage, peak power density, and impedance. The h-Mn_3O_4/CC cathode (Figure 4a) yielded 0.45 V in cathodic potential (vs Ag/AgCl), resulting in an overall MFC potential of 0.225 V in the full cell configuration. These values were significantly greater than the control based on a bare CC cathode (~0.00 V). The current density profiles with h-Mn_3O_4/CC increased over time. The current density was relatively low for the first 22 days, peaked on day 23, and then remained stable for the entire test duration of 105 days (Figure 4a). This confirms the stability of the ink over the entire test duration (105 days). The peak power density (PD) with the h-Mn_3O_4/CC electrode (75 mW·m^{-2}) was 20-fold higher compared with the control (3.75 mW·m^{-2}) (Figure 4b).

Next, we assessed if the other coated electrodes, including h-Mn_3O_4/CP, h-Mn_3O_4/RVC, and h-Mn_3O_4/felt, display similar outstanding ORR performances. The PD in the MFC with h-Mn_3O_4/CP electrode (674.58 mW·m^{-2}) was 180-fold higher than the bare CC control (3.75 mW·m^{-2}) (Figure 4b). The h-Mn_3O_4/RVC electrode yielded a PD of 58.2 mW·m^{-2}, which is 15.5-fold higher than that of bare CC. h-Mn_3O_4/felt also yielded a PD (50.2 mW·m^{-2}) that is 13.4-fold higher. As shown in Figure 4b and Figure S6 (Supporting Information) under identical polarization conditions, the MFCs with the h-Mn_3O_4/CC, h-Mn_3O_4/RVC, h-Mn_3O_4/felt, and h-Mn_3O_4/CP electrodes also yielded a stable performance throughout the test duration.

The PD with the h-Mn_3O_4/CP electrode (674.58 mW m^{-2}) was ninefold higher compared with h-Mn_3O_4/CC (75 mW·m^{-2}) (Figure 4b). We attribute this to the greater catalytic activity of the h-Mn_3O_4/CP electrode, as evident from the lower charge transfer resistance (R_{ct}) compared to control, based on the EIS tests (Figure 4c,d). The R_{ct} value, as indicated by the diameter of the semicircle in the Nyquist curve, was lower for h-Mn_3O_4/CP compared to h-Mn_3O_4/CC. The R_{ct} values for h-Mn_3O_4/CP (5.323 Ω cm^2) were 13- and 100-fold lower compared with h-Mn_3O_4/CC (66.56 Ω cm^2) and control (536.8 Ω cm^2) (see Table 2). These lower R_{ct} values suggest that the ink greatly enhances the ORR rate activity with higher electron-transfer efficiency, primarily due to greater catalyst surface area and conductivity. All the R_{ct} values were obtained by fitting the electrical equivalent circuit

https://doi.org/10.1021/acsomega.1c06950
ACS Omega 2022, 7, 11777–11787

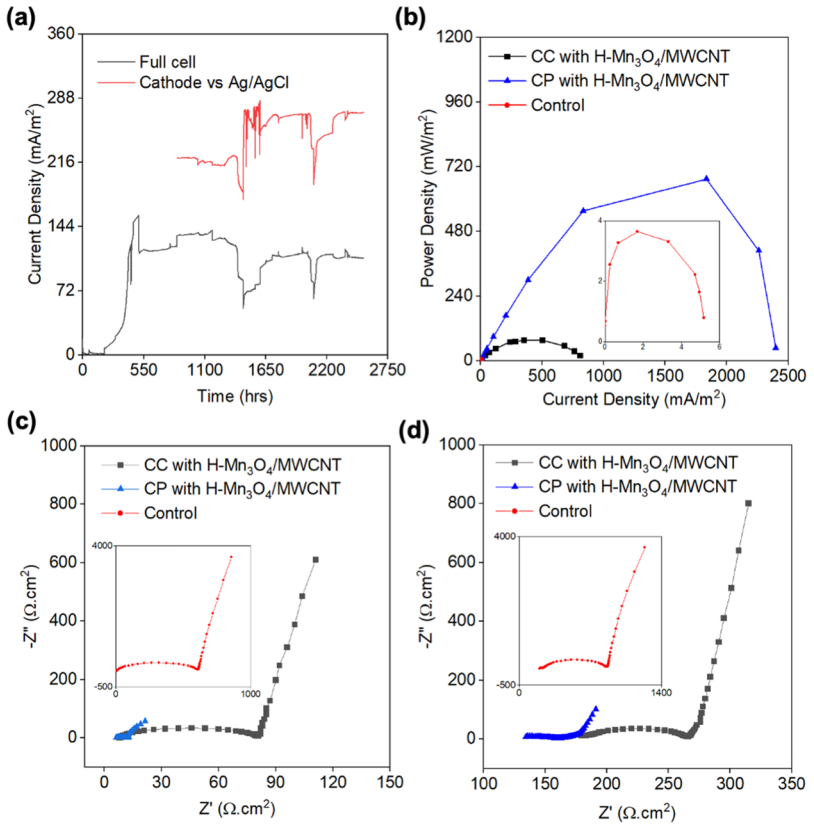

Figure 4. Performance of MFC equipped with the h-Mn_3O_4/CC and h-Mn_3O_4/carbon paper. The controls are devoid of the catalyst ink. (a) Temporal variation of cathodic and full cell current density. (b) Current density vs power density (day 92) and (c) Nyquist curve of EIS test for MFC with respect to cathode (day 92) (d) Nyquist curve of EIS test for MFC with respect to full cell (day 92) (total duration = 106 days).

Table 2. Resistance Values Obtained by Fitting Electrical Equivalent Circuit to Nyquist Plot of MFC Operated in Half-Cell Mode (Cathode as Working Electrode and Ag/AgCl as Counter and Reference Electrode)

cathode	R_s ($\Omega \cdot cm^2$)	R_{ct} ($\Omega \cdot cm^2$)
bare carbon cloth (control)	6.757	536.8
h-Mn_3O_4/CC	8.743	66.56
h-Mn_3O_4/CP (pH 4)	20.73	12.18
h-Mn_3O_4/CP (pH 7)	6.63	5.323
h-Mn_3O_4/CP (pH 13)	5.423	4.837

(Figure S2, Supporting Information) to the data from the Nyquist plots.

The higher performance with h-Mn_3O_4/CP was due to the higher surface loading rate of the h-Mn_3O_4/MWCNT ink (~2%) on the CP due to its nonporous surface. Also, the loading of h-Mn_3O_4/MWCNT ink onto the CP made the electrode super hydrophilic. The hydrophilic surfaces are known to enhance the ORR rate by increasing the adsorption, enriching the reactants onto the electrode surface.[21] Table 3 demonstrates that none of the prior MFC studies based on the MnO catalysts were based on extreme pH conditions. The performance of h-Mn_3O_4/MWCNT ink was far superior to other catalysts under extreme pH conditions and equivalent or better at the neutral pH conditions.

Performance of the Ink under Extreme pH Conditions in MFCs. Here, we demonstrate the ORR performance of h-Mn_3O_4/CP cathode under extreme acidic and alkaline conditions. In the RDE tests, the h-Mn_3O_4/MWCNT ink displayed its affinity to promote a four-electron-transfer mechanism. Here, we analyze the performance of h-Mn_3O_4/CP electrodes under extreme pH conditions (Figure 5). The coated electrodes displayed stable ORR performance at three diverse pH conditions. Their performance was higher than the uncoated electrodes, which is evident from the higher values of current density and PD (Figure 5a). We observed slight performance differences between the acidic and alkaline conditions. The OCV values at pH of 4.0 and 13 were 893 and 621.1 mV, respectively, which are different from neutral conditions (857.6 mV). Thermodynamically, the electrode potential changes by 0.059 V per unit pH change, evident from the greater OCV values at lower pH conditions (Figure 5d).[38] The potential losses due to an increase in pH affected the overall electrochemical performance of the MFCs.

Considering the higher OCV at acidic conditions, one can expect the enhanced performance of MFC; however, the overall electrochemical performance was lower at acidic conditions. The PD under the acidic conditions (462.34 mW m^{-2}) reduced slightly when compared with the neutral condition (675 mW m^{-2}) (Figure 5c). The peak current density at the acidic conditions (1854.4 mA m^{-2}) was lower than neutral (2397.5 mA m^{-2}) and alkaline conditions (2489 mA m^{-2}). The lower performance under the acidic conditions corroborates the findings of the RDE tests (Figure 3). This decreased performance was due to the higher impedance under the acidic conditions. The charge transfer resistance (12.18 ohm·cm^2) increased by ~10-fold higher compared with the neutral conditions (2.323 ohms·cm^2) (Table 2). The higher impedance can be attributed to the catalyst fouling, likely by the intermediate products, as indicated by the inductance loop

https://doi.org/10.1021/acsomega.1c06950
ACS Omega 2022, 7, 11777−11787

Table 3. Performance of h-Mn_3O_4/MWCNT Ink Compared to Other MnO Catalysts in MFC Applications

cathode material	catalyst	synthesis method	application	pH for ORR	peak power density	electron transfer	ref
carbon cloth	MnO_x/C	chemical oxidation	aqueous air-cathode	13	161 mW·m^{-2a}	4	32
carbon cloth	α-MnO_2	hydrothermal process	air-cathode	7	125 mW·m^{-2a}	NA	12
	β-MnO_2				172 mW·m^{-2a}		
	γ-MnO_2				88 mW·m^{-2a}		
polyacrylonitrile carbon felt	MnO_2/CNT	sonochemical-coprecipitation	air-cathode	NA	215 mW·m^{-3a}	NA	33
carbon paper	MnO_2-graphene nanosheet	redox reactions and microwave irradiation	air-cathode	7	2083 mW·m^{-2}	NA	34
carbon cloth	Co-doped octahedral molecular sieve MnO_2	hydrothermal process	air-cathode	NA	180 mW·m^{-2a}	NA	35
carbon paper	nano-structured MnO_x	electrochemical deposition	air-cathode	NA	772 mW·m^{-3}	NA	36
carbon cloth	MnO_2/polypyrrole	hydrothermal process	air-cathode	13	721 mW·m^{-2}	4	37
carbon paper	MnO_2/functionalized CNT	redox between functionalized CNT $KmnO_4$	aqueous air-cathode	NA	520 mW·m^{-2a}	NA	11
carbon nanofoam paper	h-Mn_3O_4/MWCNT	Kirkendall effect	aqueous air-cathode	4	462 mW·m^{-2a}	4	this study
carbon nanofoam paper	h-Mn_3O_4/MWCNT	Kirkendall effect	aqueous air-cathode	7	675 mW·m^{-2a}	4	this study
carbon nanofoam paper	h-Mn_3O_4/MWCNT	Kirkendall effect	aqueous air-cathode	13	392 mW·m^{-2a}	2	this study
carbon cloth	h-Mn_3O_4/MWCNT	Kirkendall effect	aqueous air-cathode	7	75 mW·m^{-2a}	4	this study

[a]Normalized with anode surface area and others based on the cathode surface area.

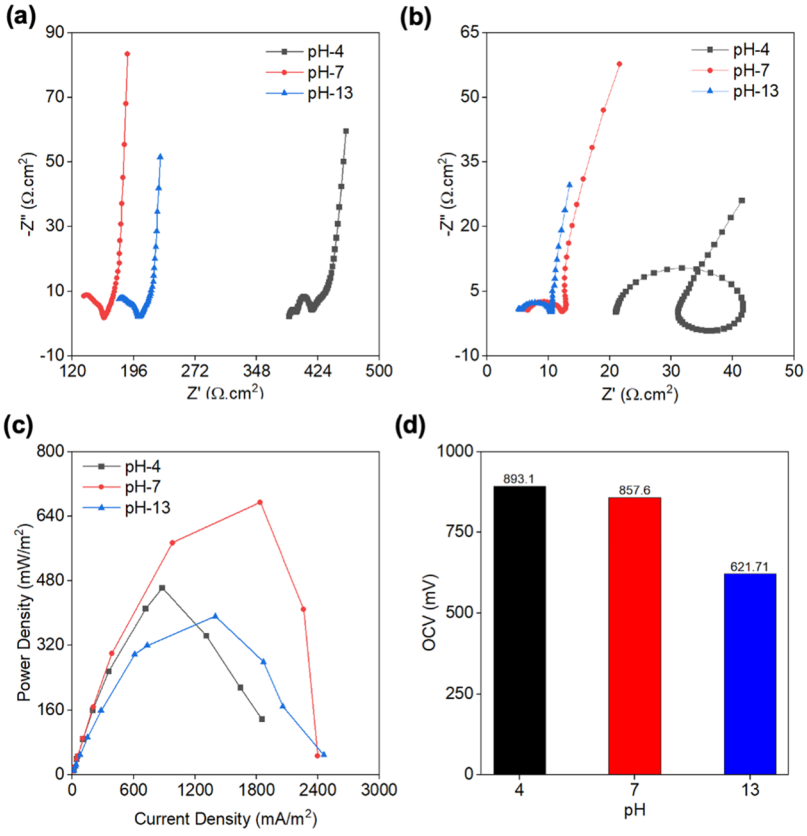

Figure 5. Performance of MFC at pH 4, pH 7, and pH 13 with h-Mn_3O_4/CP as cathode: (a) EIS of the full cell, (b) EIS of cathode, (c) power density, and (d) open-circuit potential.

in the lower frequency at pH 4.0 (Figure 5b).[39,40] The pourbaix diagram for manganese also shows the dissolution of Mn_xO_x into Mn^{2+} under acidic conditions.[41]

Under the alkaline conditions (391.68 mW m^{-2} and 2489 mA m^{-2}), the PD and current density were only slightly lower than neutral conditions (675 mW·m^{-2}, 2398 mA·m^{-2}),

https://doi.org/10.1021/acsomega.1c06950
ACS Omega 2022, 7, 11777−11787

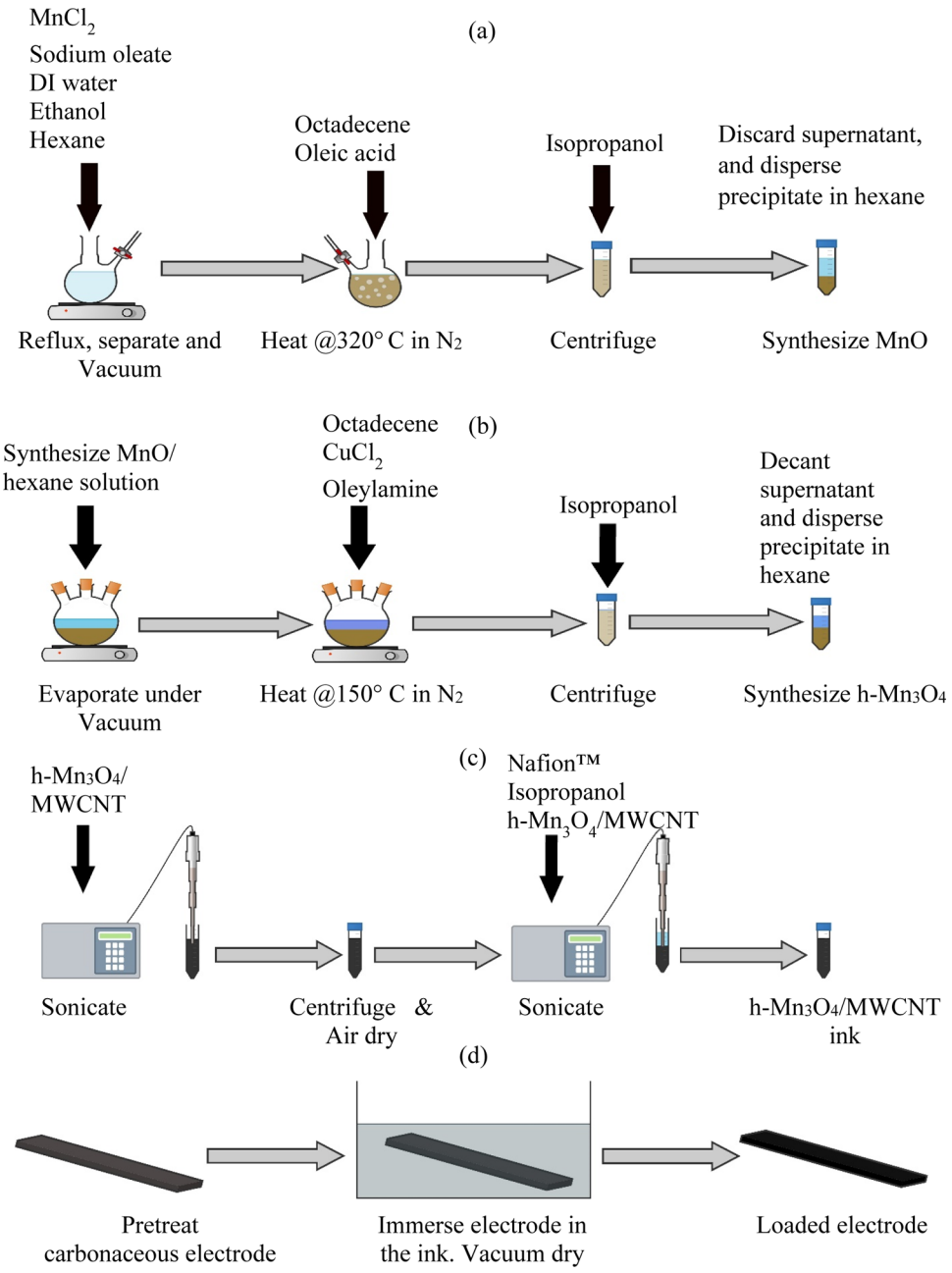

Figure 6. Synthesis of (a) MnO, (b) h-Mn_3O_4, (c) h-Mn_3O_4/MWCNT catalyst ink, and (d) electrodes modified with the catalyst ink.

respectively. The alkaline conditions in the catholyte (pH 13) resulted in a greater flux of alkali cations (K^+), combined with greater consumption of the protons for ORR, decreasing the current proton availability to the cathode.[42]

Underlying ORR Mechanisms of h-Mn_3O_4/MWCNT Catalyst Ink.

$$O_2 + 2H_2O + 4e^- \rightarrow 4OH^- \quad (1)$$

$$O_2 + * \rightarrow O_{2(ads)} \quad (2)$$

$$O_{2(ads)} + H_2O + e^- \rightarrow OOH_{(ads)} + OH^- \quad (3)$$

$$OOH_{(ads)} + e^- \rightarrow O_{(ads)} + OH^- \quad (4)$$

$$O_{(ads)} + H_2O + e^- \rightarrow OH_{(ads)} + OH^- \quad (5)$$

$$OH_{(ads)} + e^- \rightarrow OH^- \quad (6)$$

Having established the outstanding ORR activity of the ink on both planar and porous forms of carbon electrodes (Figures 3 and 4), we turn our attention onto the mechanistic possibilities of ORR using the following steps: (a) diffusion and adsorption of O_2 molecules onto the h-Mn_3O_4/MWCNT catalytic sites at the cathode (eq 2), (b) electron transport from the MFC circuit onto the adsorbed O_2 on the cathode (eq 3), (c) weakening and splitting of O═O binding by h-Mn_3O_4, (eq 3), and (d) removal of the as-produced OH^- ions (eqs 3−6).[43−45] The overall four-electron ORR that we observed in the RDE tests (eq 1) occurs by a direct pathway or a series pathway involving a peroxide intermediate. The direct pathway proceeds through a sequence of eqs 2−5 in such a way that all the four electrons from eq 1 occur on the same catalytic site. Based on the series pathway in eqs 2−6,[46−51] eq

https://doi.org/10.1021/acsomega.1c06950
ACS Omega 2022, 7, 11777−11787

3 can occur on the carbon electrode support onto which h-Mn_3O_4 is deposited or on Mn(IV) sites of h-Mn_3O_4. The catalytic activity for eq 6 is attributed to h-Mn_3O_4,[46,47,51−58] and primarily to the higher valence state of Mn(IV) species.[59−61] The hollow structure increases the catalyst site area for the ORR reactions to take place.

The stable performance of the ink for ∼106 days and on all the four porous carbon electrodes demonstrates the following unique roles of the ink. They resolve the issues with the significant volume changes, poor electrical conductivity, and low ORR current of h-Mn_3O_4 nanoparticles under ambient conditions[62] that prevail in MFCs. The MWCNT supports anchor the h-Mn_3O_4 nanoparticle while enhancing the accessible surface area for their loading (Figure S4, Supporting Information) and promoting the charge transfer (i.e., electrons and protons) to meet and reduce the terminal electron acceptors (i.e., oxygen) onto the catalyst surface. Nafion served as a proton-conducting binder to tightly adhere the h-Mn_3O_4 with MWCNT, as shown in the SEM images (Figure S4, Supporting Information).[17] The high surface area, thin walls, and hollow interior of h-Mn_3O_4 imparted the electrode materials with a larger electrode−electrolyte contact area, reduced diffusion path, as well as free interior space for alleviating structural strain and volume expansion. Altogether, we achieved a high surface coverage of h-Mn_3O_4 by deeply integrating them within the hierarchical pores of the network covered with the MWCNT on the 3D carbon electrodes. For example, as shown in the SEM and optical microscopy images (Figure S4, Supporting Information), the MWCNTs anchor h-Mn_3O_4 onto the carbon electrode surfaces, and the h-Mn_3O_4/MWCNT particles are uniformly distributed without any signs of aggregates.

■ CONCLUSIONS

This study demonstrated a proof of concept regarding the stable ORR performances of h-Mn_3O_4/MWCNT ink under extreme pH conditions in MFCs. We attribute this outstanding performance to the unique electronic and morphological properties of the h-Mn_3O_4 nanospheres. Their amenability to functionalization with MWCNTs and the ease of drop-casting the ink demonstrate the scalability prospects. We have demonstrated the long-term and stability and longevity of the ink on cathodes in real MFC for ∼105 days. The ink yielded extremely high open-circuit voltage (OCV) (893 mV, pH 4; 857.6 mV, pH 7; and 621.1 mV, pH-13), equivalent or better than platinum-based materials. The closed-circuit performance was also superior compared with the catalysts based on earth-abundant metals. Overall, the current study indicates promise for using the ink to sustain ORRs in large-scale MFC applications, including photosynthetic MFCs. The current study opens a new research direction for designing ORR reactions in MFCs to treat waste streams (e.g., mining wastes) that emerge at extreme pH conditions.

■ METHODS

Synthesis of the Catalyst Ink. Figure 6a−d depicts an overview of the synthesis of MnO, h-Mn_3O_4 nanocrystals, catalyst ink, and coated electrodes (discussed below). A detailed synthesis of MnO particles is described in the supplementary section.

Synthesis of h-Mn_3O_4 Nanoparticles. The h-Mn_3O_4 nanoparticles were prepared as described in the literature.[17] Briefly, MnO (180 mg, 2.53 mmol) was introduced into a three-neck round-bottom flask, and the hexane (6 mL) was evaporated under a vacuum. To this, 20 mL of degassed 1-octadecene and $CuCl_2·2H_2O$ were added. Degassed oleylamine was added to achieve an N:Cu ratio of 12:1. The flask was fitted with a reflux condenser, and N_2 was passed into the flask to blanket the solvent. The reaction mixture was heated to 150 °C at a rate of 10 °C/min and kept at that temperature for 3 h and then cooled to room temperature. Then, 25 mL of isopropanol was added to the cooled mixture, and the product was centrifuged at 3500 rpm for 8 min. The precipitated nanoparticles, typically dark brown, were collected, and the supernatant was discarded (Figure 6b).

Synthesis of the Ink. Details on combining h-Mn_3O_4, MWCNT and Nafion binder for obtaining a stock solution of the ink has been described in our earlier works (ref 18) (Figure 6 (referred to as ink or catalyst ink).

Deposition of the h-Mn_3O_4/MWCNT Ink on Carbon Electrodes. *GC Electrode for RDE Tests.* Prior to the application of the ink, a GC electrode was polished sequentially using three different alumina slurries (0.05, 0.3, and 5 μm suspensions, respectively) and sonicated in distilled water for 5 min (40 kHz, Branson 2510 water bath). The ink was drop cast onto the treated GC surface and air-dried for 5 min. The modified GC electrode was used in the RDE studies (see the RDE Tests section).

Porous Carbon Electrode for MFC Tests. GF, RVC, carbon cloth (CC), and carbon paper (CP) electrodes were coated with the ink to obtain ORR cathodes for the MFC studies. These electrodes were cleaned with acetone and ammonium peroxydisulfate and heated at 450 °C for 30 min.[63,64] The pretreated electrodes were washed with distilled water thrice and immersed in the ink. The mass of the ink was adjusted to be ∼5% of the equivalent mass of the electrode. The ink turned colorless after the nanoparticles were transferred onto the electrodes. The coated electrodes were dried in a vacuum oven at 200 °C (see Figure 6d). The morphology of nanoparticles coverage on the electrode surfaces and their morphology were assessed using scanning electron microscopy (SEM), Raman spectroscopy (ffTA Foram X3 module [Foster + Freeman Ltd., Evesham, UK] with 10× magnification, laser excitation wavelength of 638 nm and power of 10 mW), and optical spectroscopy.[65] Contact angle measurements were carried out using a Goniometer (Model 500, ramé-hart Instrument Co.) and DROP-image advanced v2.4 software. An ICP-AES technique was used to carry out the elemental analysis of the attached nanoparticles.

RDE Tests (Abiotic Conditions). A Pine Research modulated speed rotator (MSR) that was integrated with a three-electrode electrochemical cell was used to carry out the RDE tests. The coated GC electrode (disk surface area = 0.196 cm^2) served as the working electrode (WE), Ag/AgCl as a reference electrode, and platinum wire as a counter electrode. The RDE tests were carried out at pH 1, 7, and 13 using 0.1 M H_2SO_4, 0.01 M KCl, and 0.1 M KOH, respectively. An uncoated electrode served as a control. Cyclic voltammetry tests were carried between −0.8 and 0 V at a scan rate of 25 mV/s and rotation speeds of 400−1600 rpm. The electrolytes were saturated with O_2 by bubbling O_2 for 15 min using a dual-port gas inlet. The O_2 flow was maintained over the electrolyte during the measurements.

MFC Tests (Biotic Conditions). The test MFCs and controls that were based on two-compartment MFCs (see ref 63) were

https://doi.org/10.1021/acsomega.1c06950
ACS Omega 2022, 7, 11777−11787

operated under the cathode limited conditions. The volume of the cathode and anode compartments was 400 mL each. A graphite brush (4 cm × 5 cm) constituted the anode and four coated electrodes the cathodes (4 cm × 4 cm rectangles). The test MFCs were operated under the cathode limited conditions to assess the ORR performances of the coated electrodes. A cation exchange membrane (CMI-7000) (Membranes International Inc.) separates the anode and cathode compartments. This membrane was soaked in a 5% NaCl solution for 12 h at room temperature prior to its use. The control MFC used a bare CC as the cathode. A titanium wire was used to connect the electrodes with the external electrical circuit. The anolyte was based on the primary clarifier effluent from the Rapid City wastewater reclamation facility supplemented with sodium acetate (3 g/L). The catholyte was based on a phosphate buffer (100 mM). The catholyte and anolyte were continuously purged with oxygen (0.1 L/min) and ultrapure nitrogen (0.1 L/min), respectively (see Figure 7). This arrangement ensured aerobic and anaerobic conditions in each of the compartments, respectively. The MFC studies were carried out at room temperature.

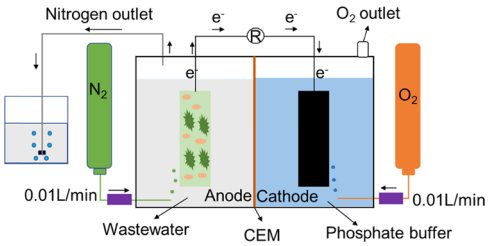

Figure 7. Two-compartment MFCs with wastewater as the anolyte, phosphate buffer as catholyte, and h-Mn_3O_4 ink as ORR catalyst on the cathode surface. The catholyte and anolyte were purged continuously with oxygen and nitrogen, respectively.

Data Acquisition and Electrochemical Analysis. Electrochemical impedance spectroscopy (EIS) tests were performed at an OCV using an alternating current (AC) signal (±10 mV) at a frequency range of 10 kHz to 0.01 Hz. A data acquisition module (DAQ/54; I/O Tech Inc., Cleveland, OH) was used to acquire the voltage data across an external load. The voltage at each resistance was measured every 30 min, and the voltage value was recorded under steady-state conditions. The EIS spectra were obtained using the cathode as the WE, anode as the counter electrode (CE), and Ag/AgCl as the reference electrode (RE). A Gamry reference 3000 workstations were used for all the EIS tests and Gamry Echem Analyst software for analyzing the impedance data. Individual resistances were obtained by external equivalent circuit (EEC) fitting analysis of the EIS data, limiting the maximum error tolerance to 2%. A modified Randle's circuit used for the EEC analyses is shown in Figure S2, Supporting Information.

■ ASSOCIATED CONTENT

Supporting Information

The Supporting Information is available free of charge at https://pubs.acs.org/doi/10.1021/acsomega.1c06950.

Detailed information on the synthesis of MnO, properties of a catalyst ink, characterization, and electrochemistry data of catalyst ink loaded commercial carbon electrodes (PDF)

■ AUTHOR INFORMATION

Corresponding Authors

James D. Hoefelmeyer − *Department of Chemistry, University of South Dakota, Vermillion, South Dakota 57069, United States;* orcid.org/0000-0002-5955-8557; Email: James.Hoefelmeyer@usd.edu

Venkataramana Gadhamshetty − *2-Dimensional Materials for Biofilm Engineering Science and Technology (2D-BEST) Center and BuGReMeDEE Consortium, South Dakota Mines, Rapid City, South Dakota 57701, United States;* orcid.org/0000-0002-8418-3515; Email: Venkata.Gadhamshetty@sdsmt.edu

Authors

Bhuvan Vemuri − *Department of Civil and Environmental Engineering, South Dakota Mines, Rapid City, South Dakota 57701, United States; BuGReMeDEE Consortium, South Dakota Mines, Rapid City, South Dakota 57701, United States*

Govinda Chilkoor − *2-Dimensional Materials for Biofilm Engineering Science and Technology (2D-BEST) Center, South Dakota Mines, Rapid City, South Dakota 57701, United States*

Pramod Dhungana − *Department of Chemistry, University of South Dakota, Vermillion, South Dakota 57069, United States*

Jamil Islam − *Department of Civil and Environmental Engineering, South Dakota Mines, Rapid City, South Dakota 57701, United States; BuGReMeDEE Consortium, South Dakota Mines, Rapid City, South Dakota 57701, United States*

Aravind Baride − *Department of Chemistry, University of South Dakota, Vermillion, South Dakota 57069, United States;* orcid.org/0000-0001-7582-1522

Nikhil Koratkar − *Department of Mechanical, Aerospace and Nuclear Engineering Rensselaer Polytechnic Institute, Troy, New York 12180, United States;* orcid.org/0000-0002-4080-3786

Pulickel M. Ajayan − *Department of Materials Science and Nano Engineering, Rice University, Houston, Texas 77005, United States;* orcid.org/0000-0001-8323-7860

Muhammad M. Rahman − *Department of Materials Science and Nano Engineering, Rice University, Houston, Texas 77005, United States;* orcid.org/0000-0003-1374-0561

Complete contact information is available at: https://pubs.acs.org/10.1021/acsomega.1c06950

Notes

The authors declare no competing financial interest.

■ ACKNOWLEDGMENTS

We acknowledge the funding support from the National Aeronautics and Space Administration (NASA #NNX16A-Q98A) and in part by the National Science Foundation CAREER award (#1454102) and NSF RII FEC awards (#1736255, #1849206, #1920954).

■ REFERENCES

(1) Li, X. M.; Cheng, K. Y.; Selvam, A.; Wong, J. W. C. Bioelectricity Production from Acidic Food Waste Leachate Using Microbial Fuel Cells: Effect of Microbial Inocula. *Process Biochem.* **2013**, *48*, 283−288.

(2) Ni, G.; Christel, S.; Roman, P.; Wong, Z. L.; Bijmans, M. F. M.; Dopson, M. Electricity Generation from an Inorganic Sulfur Compound Containing Mining Wastewater by Acidophilic Microorganisms. *Res. Microbiol.* **2016**, *167*, 568−575.
(3) Kim, H.; Kim, B.; Kim, J.; Lee, T.; Yu, J. Electricity Generation and Microbial Community in Microbial Fuel Cell Using Low-PH Distillery Wastewater at Different External Resistances. *J. Biotechnol.* **2014**, *186*, 175−180.
(4) Naik, S.; Jujjavarappu, S. E. Simultaneous Bioelectricity Generation from Cost-Effective MFC and Water Treatment Using Various Wastewater Samples. *Environ. Sci. Pollut. Res.* **2020**, *27*, 27383−27393.
(5) Shrestha, N.; Chilkoor, G.; Vemuri, B.; Rathinam, N.; Sani, R. K.; Gadhamshetty, V. Extremophiles for Microbial-Electrochemistry Applications: A Critical Review. *Bioresour. Technol.* **2018**, *255*, 318−330.
(6) Ramaswamy, N.; Mukerjee, S.; Jaksic, M. M. Fundamental Mechanistic Understanding of Electrocatalysis of Oxygen Reduction on Pt and Non-Pt Surfaces: Acid versus Alkaline Media. *Adv. Phys. Chem.* **2012**, *2012*, 17.
(7) Firouzjaie, H. A.; Mustain, W. E. Catalytic Advantages, Challenges, and Priorities in Alkaline Membrane Fuel Cells. *ACS Catal.* **2020**, 225−234.
(8) Bikkarolla, S. K.; Yu, F.; Zhou, W.; Joseph, P.; Cumpson, P.; Papakonstantinou, P. A Three-Dimensional Mn3O4 Network Supported on a Nitrogenated Graphene Electrocatalyst for Efficient Oxygen Reduction Reaction in Alkaline Media. *J. Mater. Chem. A* **2014**, *2*, 14493−14501.
(9) Luo, Y.; Zhang, H.; Wang, L.; Zhang, M.; Wang, T. Fixing Graphene-Mn3O4 Nanosheets on Carbon Cloth by a Poles Repel-Assisted Method to Prepare Flexible Binder-Free Electrodes for Supercapacitors. *Electrochim. Acta* **2015**, *180*, 983−989.
(10) Wang, Y. G.; Cheng, L.; Li, F.; Xiong, H. M.; Xia, Y. Y. High Electrocatalytic Performance of Mn3O4/Mesoporous Carbon Composite for Oxygen Reduction in Alkaline Solutions. *Chem. Mater.* **2007**, *19*, 2095−2101.
(11) Liew, K. B.; Wan Daud, W. R.; Ghasemi, M.; Loh, K. S.; Ismail, M.; Lim, S. S.; Leong, J. X. Manganese Oxide/Functionalised Carbon Nanotubes Nanocomposite as Catalyst for Oxygen Reduction Reaction in Microbial Fuel Cell. *Int. J. Hydrogen Energy* **2015**, *40*, 11625−11632.
(12) Zhang, L.; Liu, C.; Zhuang, L.; Li, W.; Zhou, S.; Zhang, J. Manganese Dioxide as an Alternative Cathodic Catalyst to Platinum in Microbial Fuel Cells. *Biosens. Bioelectron.* **2009**, *24*, 2825−2829.
(13) Liang, Y.; Li, Y.; Wang, H.; Dai, H. Strongly Coupled Inorganic/Nanocarbon Hybrid Materials for Advanced Electrocatalysis. *J. Am. Chem. Soc.* **2013**, *135*, 2013−2036.
(14) Seo, W. S.; Jo, H. H.; Lee, K.; Kim, B.; Oh, S. J.; Park, J. T. Size-Dependent Magnetic Properties of Colloidal Mn3O4 and MnO Nanoparticles. *Angew. Chem., Int. Ed.* **2004**, *43*, 1115−1117.
(15) Zhao, N.; Nie, W.; Liu, X.; Tian, S.; Zhang, Y.; Ji, X. Shape- and Size-Controlled Synthesis and Dependent Magnetic Properties of Nearly Monodisperse Mn3O4 Nanocrystals. *Small* **2008**, *4*, 77−81.
(16) Li, Y.; Tan, H.; Yang, X. Y.; Goris, B.; Verbeeck, J.; Bals, S.; Colson, P.; Cloots, R.; Van Tendeloo, G.; Su, B. L. Well Shaped Mn3O4 Nano-Octahedra with Anomalous Magnetic Behavior and Enhanced Photodecomposition Properties. *Small* **2011**, *7*, 475−483.
(17) Varapragasam, S. J. P.; Balasanthiran, C.; Gurung, A.; Qiao, Q.; Rioux, R. M.; Hoefelmeyer, J. D. Kirkendall Growth of Hollow Mn3O4 Nanoparticles upon Galvanic Reaction of MnO with Cu2+ and Evaluation as Anode for Lithium-Ion Batteries. *J. Phys. Chem. C* **2017**, *121*, 11089−11099.
(18) Dhungana, P.; Varapragasam, S. J. P.; Vemuri, B.; Baride, A.; Shrestha, N.; Balasingam, M.; Gadhamshetty, V.; Koppang, M. D.; Hoefelmeyer, J. D. A PH-Universal Hollow-Mn3O4/MWCNT/Nafion Modified Glassy Carbon Electrode for Electrochemical Oxygen Reduction. *ChemElectroChem* **2021**, *8*, 1775−1783.
(19) Mariappan, R.; Ponnuswamy, V.; Suresh, P. Effect of Doping Concentration on the Structural and Optical Properties of Pure and Tin Doped Zinc Oxide Thin Films by Nebulizer Spray Pyrolysis (NSP) Technique. *Superlattices Microstruct.* **2012**, *52*, 500−513.
(20) Silva, G. C.; Almeida, F. S.; Dantas, M. S. S.; Ferreira, A. M.; Ciminelli, V. S. T. Raman and IR Spectroscopic Investigation of As Adsorbed on Mn_3O_4 Magnetic Composites. *Spectrochim. Acta, Part A* **2013**, *100*, 161−165.
(21) Li, T.; Wang, J.; Wang, F.; Zhang, L.; Jiang, Y.; Arandiyan, H.; Li, H. The Effect of Surface Wettability and Coalescence Dynamics in Catalytic Performance and Catalyst Preparation: A Review. *ChemCatChem* **2019**, *11*, 1576−1586.
(22) Liu, X.; Xu, W.; Zheng, D.; Li, Z.; Zeng, Y.; Lu, X. Carbon Cloth as an Advanced Electrode Material for Supercapacitors: Progress and Challenges. *J. Mater. Chem. A* **2020**, *8*, 17938−17950.
(23) Manocha, L. M. Carbon Fibers. *Encycl. Mater. Sci. Technol.* **2001**, 906−916.
(24) Zhao, Y.; Ma, Y.; Li, T.; Dong, Z.; Wang, Y. Modification of Carbon Felt Anodes Using Double-Oxidant HNO3/H2O2 for Application in Microbial Fuel Cells. *RSC Adv.* **2018**, *8*, 2059−2064.
(25) Castañeda, L. F.; Walsh, F. C.; Nava, J. L.; Ponce de León, C. Graphite Felt as a Versatile Electrode Material: Properties, Reaction Environment, Performance and Applications. *Electrochim. Acta* **2017**, *258*, 1115−1139.
(26) CeraMaterials. GFE-1 Graphite Felt (TDS).
(27) Carbon & Graphite Felt. https://www.graphite-eng.com/uploads/downloads/carbon_and_graphite_felt.pdf (accessed August 13, 2021).
(28) Duocel Reticulated Vitreous Carbon (RVC) Foam − ERG Aerospace. http://ergaerospace.com/materials/duocel-reticulated-vitreous-carbon-rvc-foam/ (accessed June 3, 2021).
(29) Friedrich, J. M.; Ponce-de-León, C.; Reade, G. W.; Walsh, F. C. Reticulated Vitreous Carbon as an Electrode Material. *J. Electroanal. Chem.* **2004**, *561*, 203−217.
(30) Ho, M. P.; Lau, A. K. T. Amorphous Carbon Nanocomposites. *Fillers Reinf. Adv. Nanocompos.* **2015**, 309−328.
(31) Carbon Nanofoam Paper. https://www.hightechmaterialsolutions.com/carbon-nanofoam-paper (accessed June 3, 2021).
(32) Roche, I.; Katuri, K.; Scott, K. A Microbial Fuel Cell Using Manganese Oxide Oxygen Reduction Catalysts. *J. Appl. Electrochem.* **2010**, *40*, 13−21.
(33) Woon, C. W.; Ong, H. R.; Chong, K. F.; Chan, K. M.; Khan, M. M. R. MnO2/CNT as ORR Electrocatalyst in Air-Cathode Microbial Fuel Cells. *Procedia Chem.* **2015**, *16*, 640−647.
(34) Wen, Q.; Wang, S.; Yan, J.; Cong, L.; Pan, Z.; Ren, Y.; Fan, Z. MnO 2-Graphene Hybrid as an Alternative Cathodic Catalyst to Platinum in Microbial Fuel Cells. *J. Power Sources* **2012**, *216*, 187−191.
(35) Li, X.; Hu, B.; Suib, S.; Lei, Y.; Li, B. Manganese Dioxide as a New Cathode Catalyst in Microbial Fuel Cells. *J. Power Sources* **2010**, *195*, 2586−2591.
(36) Liu, X. W.; Sun, X. F.; Huang, Y. X.; Sheng, G. P.; Zhou, K.; Zeng, R. J.; Dong, F.; Wang, S. G.; Xu, A. W.; Tong, Z. H.; Yu, H. Q. Nano-Structured Manganese Oxide as a Cathodic Catalyst for Enhanced Oxygen Reduction in a Microbial Fuel Cell Fed with a Synthetic Wastewater. *Water Res.* **2010**, *44*, 5298−5305.
(37) Yuan, H.; Deng, L.; Tang, J.; Zhou, S.; Chen, Y.; Yuan, Y. Facile Synthesis of MnO2/Polypyrrole/MnO2 Multiwalled Nanotubes as Advanced Electrocatalysts for the Oxygen Reduction Reaction. *ChemElectroChem* **2015**, *2*, 1152−1158.
(38) Clauwaert, P.; Aelterman, P.; Pham, T. H.; De Schamphelaire, L.; Carballa, M.; Rabaey, K.; Verstraete, W. Minimizing Losses in Bio-Electrochemical Systems: The Road to Applications. *Appl. Microbiol. Biotechnol.* **2008**, *79*, 901−913.
(39) Aricò, A.; Alderrucci, V.; Antonucci, V.; Ferrara, S.; Recupero, V.; Giordano, N.; Kinoshita, K. Ac Impedance Spectroscopy of Porous Gas Diffusion Electrode in Sulphuric Acid. *Electrochim. Acta* **1991**, *36*, 1979−1984.
(40) Bai, L.; Conway, B. E. AC Impedance of Faradaic Reactions Involving Electrosorbed Intermediates: Examination of Conditions

https://doi.org/10.1021/acsomega.1c06950
ACS Omega 2022, 7, 11777−11787

Leading to Pseudoinductive Behavior Represented in Three-Dimensional Impedance Spectroscopy Diagrams. *J. Electrochem. Soc.* **1991**, *138*, 2897−2907.
(41) Yi, C. P.; Majid, S. R. The Electrochemical Performance of Deposited Manganese Oxide-Based Film as Electrode Material for Electrochemical Capacitor Application; In *Semiconductors − Growth and Characterization*; InTech, 2018. DOI: 10.5772/intechopen.71957.
(42) Zhao, F.; Harnisch, F.; Schröder, U.; Scholz, F.; Bogdanoff, P.; Herrmann, I. Challenges and Constraints of Using Oxygen Cathodes in Microbial Fuel Cells. *Environ. Sci. Technol.* **2006**, *40*, 5193−5199.
(43) Cao, R.; Lee, J.-S.; Liu, M.; Cho, J. Recent Progress in Non-Precious Catalysts for Metal-Air Batteries. *Adv. Energy Mater.* **2012**, *2*, 816−829.
(44) Wang, Z.-L.; Xu, D.; Xu, J.-J.; Zhang, X.-B. Oxygen Electrocatalysts in Metal−Air Batteries: From Aqueous to Nonaqueous Electrolytes. *Chem. Soc. Rev.* **2014**, *43*, 7746−7786.
(45) Ma, R.; Lin, G.; Zhou, Y.; Liu, Q.; Zhang, T.; Shan, G.; Yang, M.; Wang, J. A Review of Oxygen Reduction Mechanisms for Metal-Free Carbon-Based Electrocatalysts. *npj Comput. Mater.* **2019**, *5*, 1−15.
(46) Mao, L.; Zhang, D.; Sotomura, T.; Nakatsu, K.; Koshiba, N.; Ohsaka, T. Mechanistic Study of the Reduction of Oxygen in Air Electrode with Manganese Oxides as Electrocatalysts. *Electrochim. Acta* **2003**, *48*, 1015−1021.
(47) Mao, L.; Sotomura, T.; Nakatsu, K.; Koshiba, N.; Zhang, D.; Ohsaka, T. Electrochemical Characterization of Catalytic Activities of Manganese Oxides to Oxygen Reduction in Alkaline Aqueous Solution. *J. Electrochem. Soc.* **2002**, *149*, A504.
(48) Yeager, E. Dioxygen Electrocatalysis: Mechanisms in Relation to Catalyst Structure. *J. Mol. Catal.* **1986**, *38*, 5−25.
(49) Cheng, F.; Su, Y.; Liang, J.; Tao, Z.; Chen, J. MnO2-Based Nanostructures as Catalysts for Electrochemical Oxygen Reduction in Alkaline Media†. *Chem. Mater.* **2009**, *22*, 898−905.
(50) Lima, F. H. B.; Calegaro, M. L.; Ticianelli, E. A. Investigations of the Catalytic Properties of Manganese Oxides for the Oxygen Reduction Reaction in Alkaline Media. *J. Electroanal. Chem.* **2006**, *590*, 152−160.
(51) Lima, F. H. B.; Calegaro, M. L.; Ticianelli, E. A. Electrocatalytic Activity of Manganese Oxides Prepared by Thermal Decomposition for Oxygen Reduction. *Electrochim. Acta* **2007**, *52*, 3732−3738.
(52) Gasteiger, H. A.; Kocha, S. S.; Sompalli, B.; Wagner, F. T. Activity Benchmarks and Requirements for Pt, Pt-Alloy, and Non-Pt Oxygen Reduction Catalysts for PEMFCs. *Appl. Catal., B* **2005**, *56*, 9−35.
(53) Xiao, W.; Wang, D.; Lou, X. W. Shape-Controlled Synthesis of MnO2 Nanostructures with Enhanced Electrocatalytic Activity for Oxygen Reduction. *J. Phys. Chem. C* **2009**, *114*, 1694−1700.
(54) Navrotsky, A.; Ma, C.; Lilova, K.; Birkner, N. Nanophase Transition Metal Oxides Show Large Thermodynamically Driven Shifts in Oxidation-Reduction Equilibria. *Science* **2010**, *330*, 199−201.
(55) Shanmugam, S.; Gedanken, A. MnO Octahedral Nanocrystals and MnO@C Core−Shell Composites: Synthesis, Characterization, and Electrocatalytic Properties. *J. Phys. Chem. B* **2006**, *110*, 24486−24491.
(56) Brenet, J. P. Electrochemical Behaviour of Metallic Oxides. *J. Power Sources* **1979**, *4*, 183−190.
(57) El-Deab, M. S.; Ohsaka, T. Electrocatalytic Reduction of Oxygen at Au Nanoparticles−Manganese Oxide Nanoparticle Binary Catalysts. *J. Electrochem. Soc.* **2006**, *153*, A1365.
(58) Gorlin, Y.; Chung, C.-J.; Nordlund, D.; Clemens, B. M.; Jaramillo, T. F. Mn3O4 Supported on Glassy Carbon: An Active Non-Precious Metal Catalyst for the Oxygen Reduction Reaction. *ACS Catal.* **2012**, *2*, 2687−2694.
(59) Tang, Q.; Jiang, L.; Liu, J.; Wang, S.; Sun, G. Effect of Surface Manganese Valence of Manganese Oxides on the Activity of the Oxygen Reduction Reaction in Alkaline Media. *ACS Catal.* **2014**, *4*, 457−463.
(60) Cao, Y. L.; Yang, H. X.; Ai, X. P.; Xiao, L. F. The Mechanism of Oxygen Reduction on MnO2-Catalyzed Air Cathode in Alkaline Solution. *J. Electroanal. Chem.* **2003**, *557*, 127−134.
(61) Liu, J.; Jiang, L.; Zhang, T.; Jin, J.; Yuan, L.; Sun, G. Activating Mn3O4 by Morphology Tailoring for Oxygen Reduction Reaction. *Electrochim. Acta* **2016**, *205*, 38−44.
(62) Logothetis, E. M.; Park, K. The Electrical Conductivity of Mn3O4. *Solid State Commun.* **1975**, *16*, 909−912.
(63) Vemuri, B.; Xia, L.; Chilkoor, G.; Jawaharraj, K.; Sani, R. K.; Amarnath, A.; Kilduff, J.; Gadhamshetty, V. Anaerobic Wastewater Treatment and Reuse Enabled by Thermophilic Bioprocessing Integrated with a Bioelectrochemical/Ultrafiltration Module. *Bioresour. Technol.* **2021**, *321*, No. 124406.
(64) Shrestha, N.; Chilkoor, G.; Xia, L.; Alvarado, C.; Kilduff, J. E.; Keating, J. J.; Belfort, G.; Gadhamshetty, V. Integrated Membrane and Microbial Fuel Cell Technologies for Enabling Energy-Efficient Effluent Re-Use in Power Plants. *Water Res.* **2017**, *117*, 37−48.
(65) Srivastava, I.; Mehta, R. J.; Yu, Z.-Z.; Schadler, L.; Koratkar, N. Raman Study of Interfacial Load Transfer in Graphene Nanocomposites. *Appl. Phys. Lett.* **2011**, *98*, 063102.

https://doi.org/10.1021/acsomega.1c06950
ACS Omega 2022, 7, 11777−11787